Optics for the 90 GHz GBT array

Introduction

The 90 GHz array will have 64 TES bolometers arranged in an 8×8 square, read out using 8 SQUID multiplexers. It is designed as a facility instrument for the GBT telescope which is an off-axis Gregorian system. The primary mirror is 100 m in diameter and the secondary is 8 m. The 90 GHz array is designed for the Gregorian focus where the f# is 1.94. This document describes cooled optics designed to couple the TES detectors to the existing GBT optics.

The work was carried out using Code V optical design software and the solution is available in Code V native format (.len), as a sequence file (.seq), or (for those with Zemax) it may be translated into Zemax format (look at the directory Seq2ZMX). Many of the tests are complex. Script files and even programs (in Code V's native language) have been written to carry them out. This way the tests are easily repeated on new designs

Requirements

The optical system for the GBT must:
- Produce a plate scale of 1.27 arcseconds/mm. This gives ~0.525f? pixel spacing on the sky from the detectors which are spaced by 3.3 mm.
- Control the illumination of the secondary and primary mirrors.
- Keep optical loading on the cryogenics within acceptable limits; <100 mW @ 40 K; <10 mW @ 3 K; and <5 µW @ 0.3 K for the cryogenics)
- Keep optical loading on the detectors below 2 pW/detector
- Define a bandpass. For the first tests this should be 86—94 GHz.
- Flexibility is needed. In the future we may want to change bandpasses, detector spacing, or detector loading.

Size restrictions

The Gregorian receivers are mounted in a receiver cabin. The roof of the cabin rotates to allow any of 8 receivers to be moved into the secondary focus (Figure 1.). The receivers are lowered through circular holes and the 90 GHz array is assigned a 24 inch diameter hole. This puts a hard limit on the size of the cryostat of 23.75 inches (603 mm) with a goal of 20 inches (508 mm). This lower goal is to allow cables to be fed through and to keep weight down.

The detectors are cooled using a 2-stage pulse-tube (~40 and ~3 K) and helium-4 and helium-3 adsorption (~0.7 and ~0.3 K) refrigerators. These three objects (cylinders ~100 mm diameter), the detector electronics (~15×150×150 mm), and the optics must fit within the cryostat with at least 30 mm room for heat shields around the edges.

Final design

A schematic of the final design is shown in Figure 2. The overall length of the optics (focus to focus) is 390 mm and they are less then 150 mm in diameter. Some notes on different parts follow:

Bare arrays are used. To obtain the 1.27 plate scale, the final focus must be f1.62. Horns can not be used as they would physically overlap (or their apertures would be too small to allow 90 GHz light through) and illumination of the telescope is controlled with a cold Lyot stop.
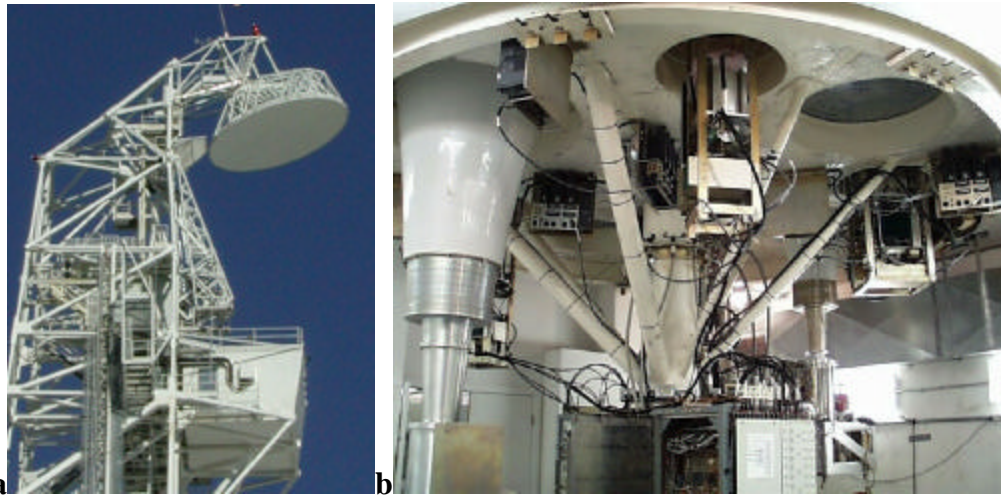
Figure 1: **a** : The 8 m secondary mirror and receiver cabin seen from below. **b** : The inside of the receiver cabin showing the holes where the 90 GHz array must fit.

The Lenses

- Both lenses are 10th order aspheres. The use of aspheres increased off-axis image quality while maintaining a good Lyot stop.
- The lenses are diamond turned out of high purity, high resistivity silicon. This material is easy to obtain and its high refractive index means lenses can be thin. Silicon has very low loss at 90 GHz. Silicon also has good thermal conductivity and can act as a secondary IR blocker.
- Because of its high refractive index anti-reflective (AR) coating the lenses is required. Cardiff University has experience putting AR coatings on silicon. These coatings made of a plastic metal-oxide mixture, tailored to give the correct refractive index, require a 5 µm finish, easily obtainable with diamond turning.
- Image quality could be easier to obtain if lens 2 is reversed but this would lead to very bad ghosting (see below) so aspheric surfaces have been used to obtain image quality instead (see ghosting section below).
- The positions of the lenses have been chosen to match the heights of the temperature stages of the pulse tube to make installation easy.

Loading and bandpass filters

- To keep loading on the cryogenics to a minimum the cryostat window is placed close to the Gregorian focus (where it can be small).
- A reflecting capacitive mesh lowpass filter at 40 K (filter 1) keeps IR power from the colder stages where less cooling power is available. Neutral density filters can also be added at this location. This could become necessary if the atmospheric emission is greater than expected. By placing these filters near to the window they are smaller, making their manufacture easier and further reducing the amount of IR-power.
- Filter 2 is also a lowpass capacitive mesh filter designed to cut out the peak of the 40K black body spectrum and stop and leaks in filter 1. It's cut off frequency should be close to the top of the band but it need not be too sharp.
- Filter 3 is the capacitive mesh bandpass filter. Its leaks are cut out by filters 1 & 2. It is important in controlling the loading on the detectors. Without it, 3 K radiation from the Lyot stop would saturate the detectors. Filter 3 reduces this loading to 0.22 pW/detector.
- The total loading from the cold optics is estimated to be 0.43 pW, compared to 0.27 pW from the warm mirrors and 0.5—2.8 pW from the atmosphere.
- The radii of the apertures (apart from the Lyot stop) have been set to 130% of the radii of the clear apertures needed to admit all the light from the rays hitting the corner of the corner

detector (v2×4×4.2?=23.7? off-axis). The sizes have been rounded up to 'nice' numbers (eg. 37.8 mm ? 40 mm). (Values in Appendix)

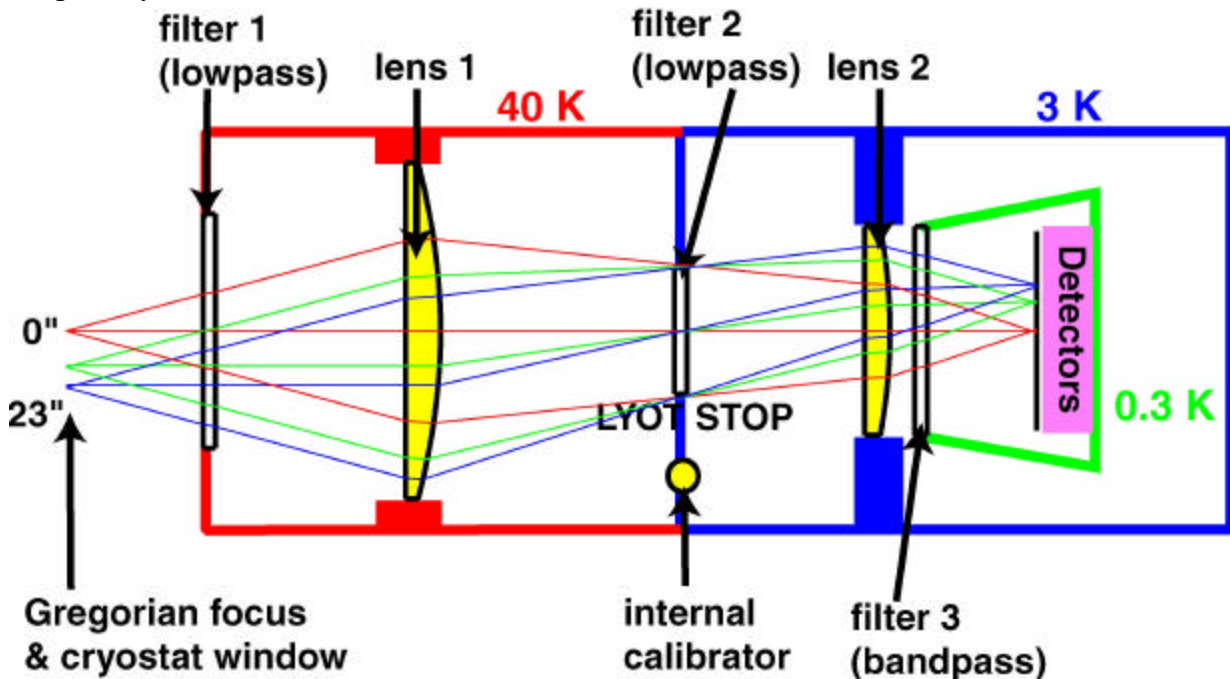- The radii of the Lyot stop has been set so that (using geometric optics) it illuminates 90 m of the primary mirror.

Figure 2. A schematic of the optical design.

Image quality

When designing the optics, the image quality was optimized simultaneously for rays 0? to 34? off-axis. 13 ray heights were used, concentrated below 23? (where our detectors will be). To create a good Lyot stop the RMS differences between the rays at its edge were calculated and added to the error function used in optimization. Getting the weight of this term was important as it was often possible to sacrifice image quality for a perfect Lyot stop. During optimization the effective focal length was constrained to be 162,000 mm exactly. After optimization the image quality was evaluated at a grid of points across the array. All points less than 27? off-axis were found to be diffraction limited to better than 1%. The finite size of the detectors causes far more change in the beam size (10 to 20%). The f# changes from f/1.595 in the center of the array to f/1.679 at the very edge.

Examples of spot diagrams and modular transfer functions (MTFs) are shown in Figure 3. Code V was used to calculate the PSF using the geometric ray tracing approximation. Beam widths were ~8? (FWHM) and the first side lobes were -17.7 dB down, 11.4? from the center of the beam. Far out side lobes dropped to below -40 dB. These calculations are approximations (due to the geometric ray tracing), better calculations were carried out using full diffraction (see below).
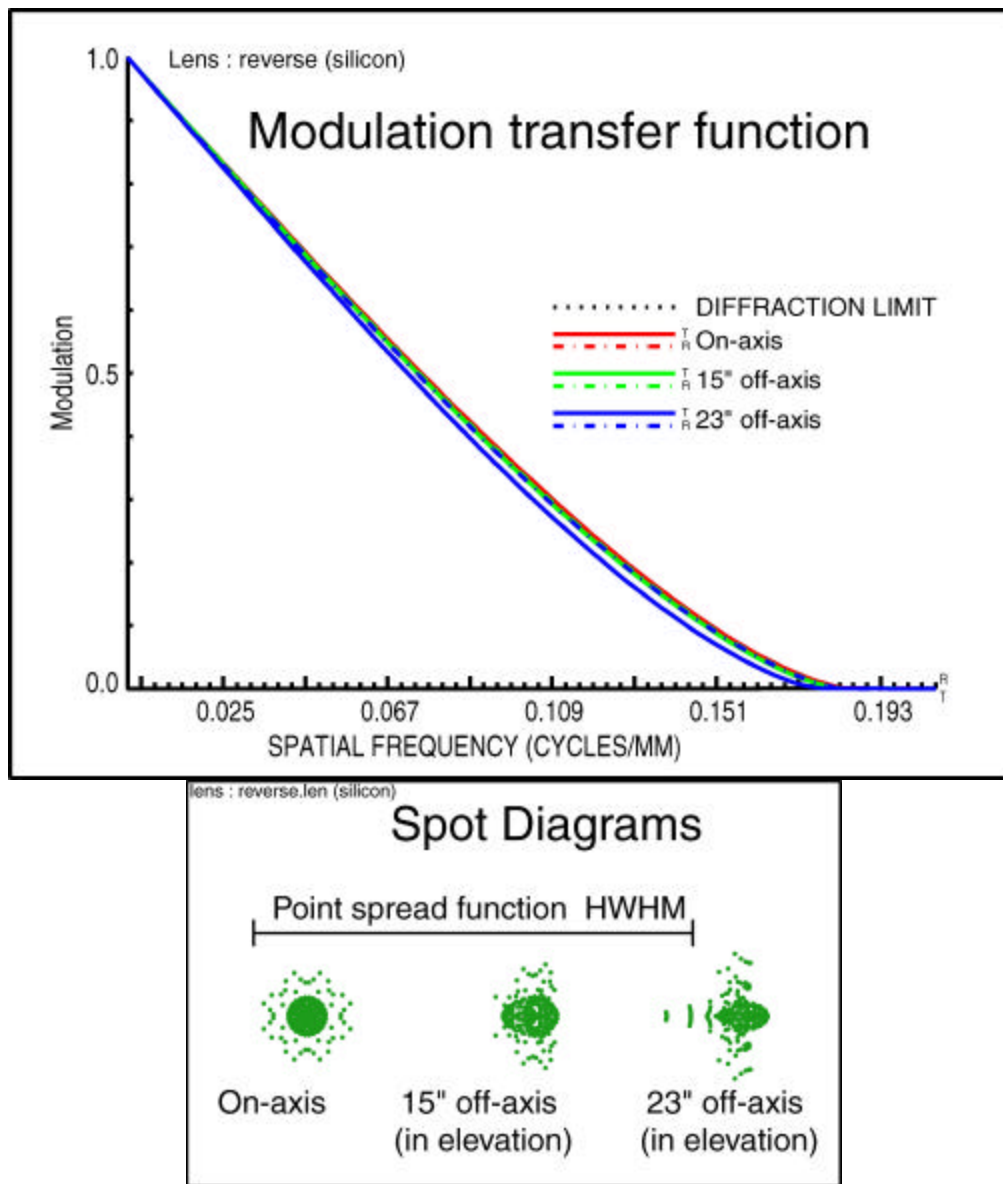
Figure 3. The spot diagrams and modular transfer functions for rays 0, 15 and 23? off-axis. The RMS spot diameters are 0.27, 0.29 and 0.35 mm respectively. The diffraction PSF has a FWHM of 6.6 mm. Some asymmetry can be seen in the 23? MTF.

Tolerancing

To check that the design is not sensitive to misalignments and manufacturing errors, inverse tolerancing was used to determine how large the errors would have to be in order to produce an RMS wavefront error of 1% (a decrease in the gain of 1.6%). The results for the on-axis pixel are in Table 1. (Some of these errors are less than 1% because the quantity being investigated had a very small effect on the RMS and Code V hit an upper limit.) Other pixels were similar. Many parameters have little or no affect on image quality. If all the errors in the table are allowed to take a random value (with a uniform distribution) between zero and the values listed, the probable (97.7%) RMS wavefront error is 2.5%, a decrease in gain of 9.4%.

Quantity	Error	RMS wavefront error
Refractive index of lens	0.04	1.0%
Refractive index of filter	0.04	0.0%

Z position of lens 1	3 mm	0.7%
Z position of Lyot stop	3 mm	0.1%
Z position of lens 2	3 mm	0.1%
Z position of array	2.8 mm	1.0%
Fit of lens 1 to test plate	0.3 mm	0.8%
Fit of lens 2 to test plate	0.3 mm	0.5%
Tilt of lens 1	6°	0.1%
Tilt of lens 2	6°	0.2%
Y Shift of lens 1	10 mm	0% (image moved off-axis)
Y Shift of lens 2	10 mm	0% (image moved off-axis)
Tilt of receiver	6°	0.2%
Y Shift of receiver	10 mm	0% (image moved off-axis)
Z Shift of receiver	4.2 mm	1.0%

Table 1 : RMS errors in the wavefronts due to misalignments. Z shifts are along the optical axis and Y shifts perpendicular.

This process was then repeated, allowing the secondary mirror to be moved (up to 2 cm & 4°) to simulate the process of focusing the telescope – a process that will be needed anyway. With the exception of tilts and displacements of the lenses is possible to focus these errors out. The expected RMS wavefront error decreased to 0.6% (a reduction in gain of less then 1%). The maximum mirror movement was 11mm and .3°. This demonstrates that manufacture and assembly of the design should not be a problem and sub-millimeter alignment is not needed.

Predicted PSF and spillover

All the above tests use geometric ray tracing. To test the effects of diffraction, the Code V model was reversed so that the source was a point on the array and a perfect lens added after the primary mirror so that a perfect telescope (which would produce plane wavefronts) would image at a point when geometric optics is used for analysis. The stop was changed to be the Lyot stop. All aperture sizes were set to be the clear apertures listed in the Appendix.

To simulate the illumination of the stop by a flat black body (whose apparent area will decrease as the cosine of the angle from the axial direction), a .int file was then placed over a dummy surface centered on the point source. Geometric ray tracing was used to calculate the phase and amplitude of the illumination across the Lyot stop. It should be noted that as the detectors are of comparable size to the wavelength, this model may not be accurate, however when no .int file was used the results of these tests showed no significant difference.

The BPR option in Code V was then used to calculate the illumination of each surface from the Lyot stop onwards (using the apertures set above). BPR uses ray tracing to calculate the amplitude and phase on a reference sphere one side of a surface from the amplitude and phase of a similar reference sphere on the other. Full diffraction calculations are then used to calculate the illumination of one surface from the last. In these calculations Code V automatically chose the diffraction regime.

From the illumination of the secondary and primary mirrors spillover and beam patterns were calculated. These are shown in Table 2. Cross-sections of the illumination of the secondary

and primary mirrors are shown in Figure 4. Both show that the illumination of the mirrors is well controlled and that ground or sky spillover will not be a problem.

Azimuth (?)	Elevation (?)	Spillover at Secondary	Spillover at primary
0	0	0.07%	0.24%
0	14.3	0.01%	0.07%
14.5	14.5	0.26%	0.33%

Table 2. Spillover from the mirrors calculated using BPR as a function of distance from the center of the array.
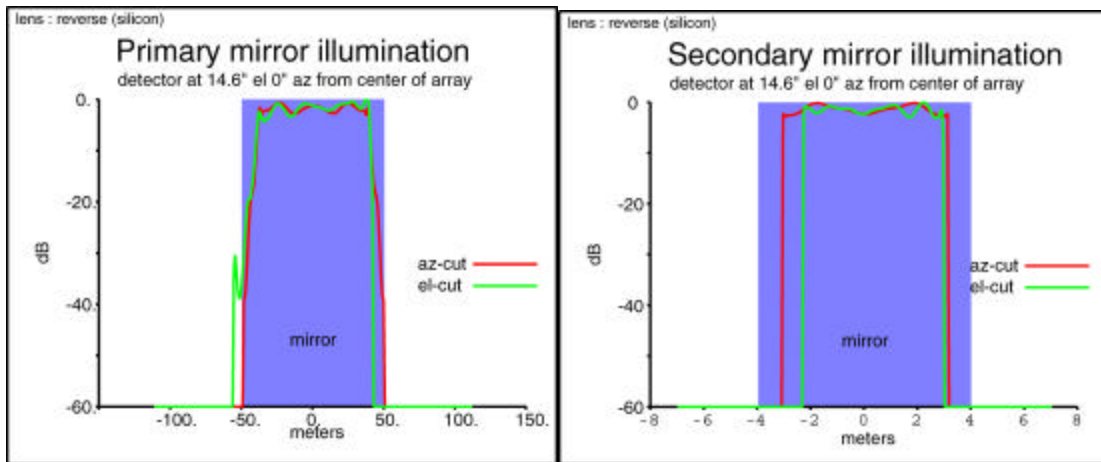

Figure 4. The illumination of the primary and secondary mirrors calculated using BPR.

By taking FFTs of the primary mirror illumination and convolving the result with the geometric image of a detector on the sky, beam patterns across the array were calculated. In order to obtain resolution, the primary was coarsely sampled in the center of a (2048×2048) FFT grid, (the largest my desktop could handle within Code V). Even so resolution was limited to 0.1?. Two examples are shown in Figure 5. FWHM were 7.9? at the center of the array and 8.05? at the edge, 1? smaller than expected from a uniformly illuminated 90 m mirror (once detector size is taken into account). Typical first side lobes are -16 dB to -18 dB down (slightly higher than expected) and far out side lobes are -35 to -40 dB down. Side lobes decreased at the very edge of the array possibly due to rounding of the illumination pattern (the beam width also showed a slight decrease here to 7.7? which would be consistent with this).
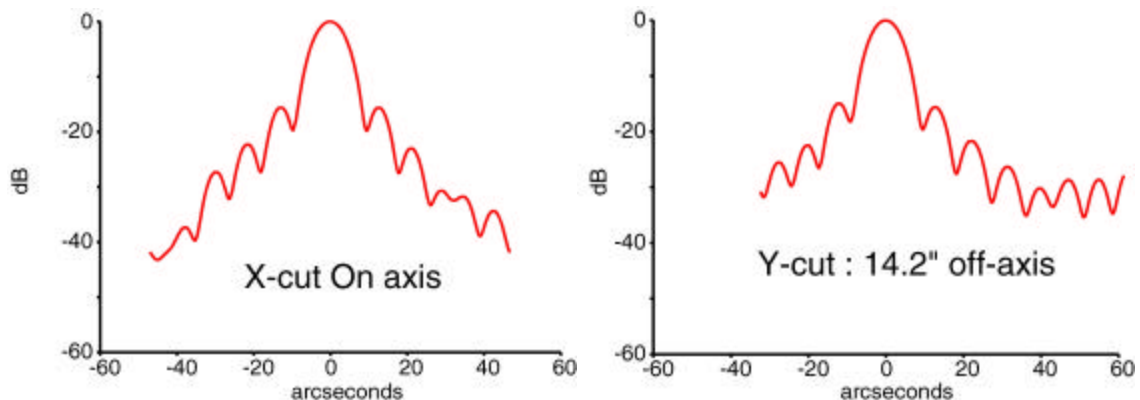

Figure 5 : Beam patterns calculated from FFTs of the primary mirror illumination. The results have been convolved with the detector's geometric image to take into account detector size.

Ghosting

The last check of the optics was to ensure stray light from reflections off surfaces does not cause any strong ghost images. Each surface was assigned a realistic reflectivity; 20% for the array and 2% for each lens or filter surface. It was assumed that the optics were in an optics box designed so that stray light is absorbed. The lens file, from the Gregorian window to a dummy surface at the array was turned into non-sequential surfaces and large edge apertures were added to each surface so that any rays that missed the clear aperture would be absorbed.

A surface near the array was made to reflect the first time a ray hits and refract the second time the same ray hits it, while another surface further from the array was made to refract first then reflect allowing Code V to model reflections between any pair of surfaces. An example where light is reflected from the array, travels out to the flat side of lens 2 before being reflected back to form an out-of-focus image is shown in Figure 6.
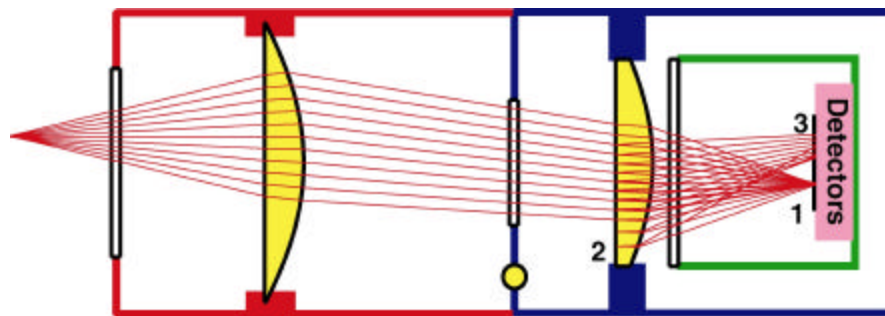

Figure 6. One of the most intense ghost images. Light is reflected off the array at 1. It hits the flat side of the second lens at 2. and creates an out-of-focus image at 3. This image is particularly strong as reflections from the array are 20% and all of this light is making it back to the array.

For each pair of surfaces the illumination of focal plane from a point source at infinity was calculated using Monte Carlo ray tracing with 10^5 rays (Code V's LUM function). The strength of the point source was set proportional to the combined reflectivity of the surfaces in question with allowances for losses at the additional number of surfaces that the rays must cross. Calculations for every pair of surfaces were added together to give the total ghost image. This was normalized by carrying out a LUM run without any surfaces reflecting and normalizing everything to the total power reaching the array. The ghost image was convolved with a 7.5? FWHM Gaussian to approximate diffraction. If this was not done then power concentrated in sharp sub-diffraction sized peaks could have masked a diffuse but still bright ghost image.

The ghosting analysis program takes about an hour to run, and has been used both on and off axis. A cut through the ghost image from a source 15? off-axis with a PSF (calculated using BEA above) superimposed on top is shown in Figure 7. As well as the total image there are plots showing the individual contributions of the different surfaces (grouped as to where the light is first reflected from). The highest image is 32 dB down but all this power comes from reflections within the filters. As a result this ghost image will always fall where the real image is and is not important. There is also a broad peak at -40 dB 12 to 38? off-axis. With the current design this is still well below the PSF and so is not a problem, even should our estimated reflectivities be too low. However if lens 2 has its curved side away from the array this peak becomes much more focused with a peak ~-29 dB (higher than some predicted diffraction side lobes). For this reason the less than ideal orientation of lens 2 was chosen.
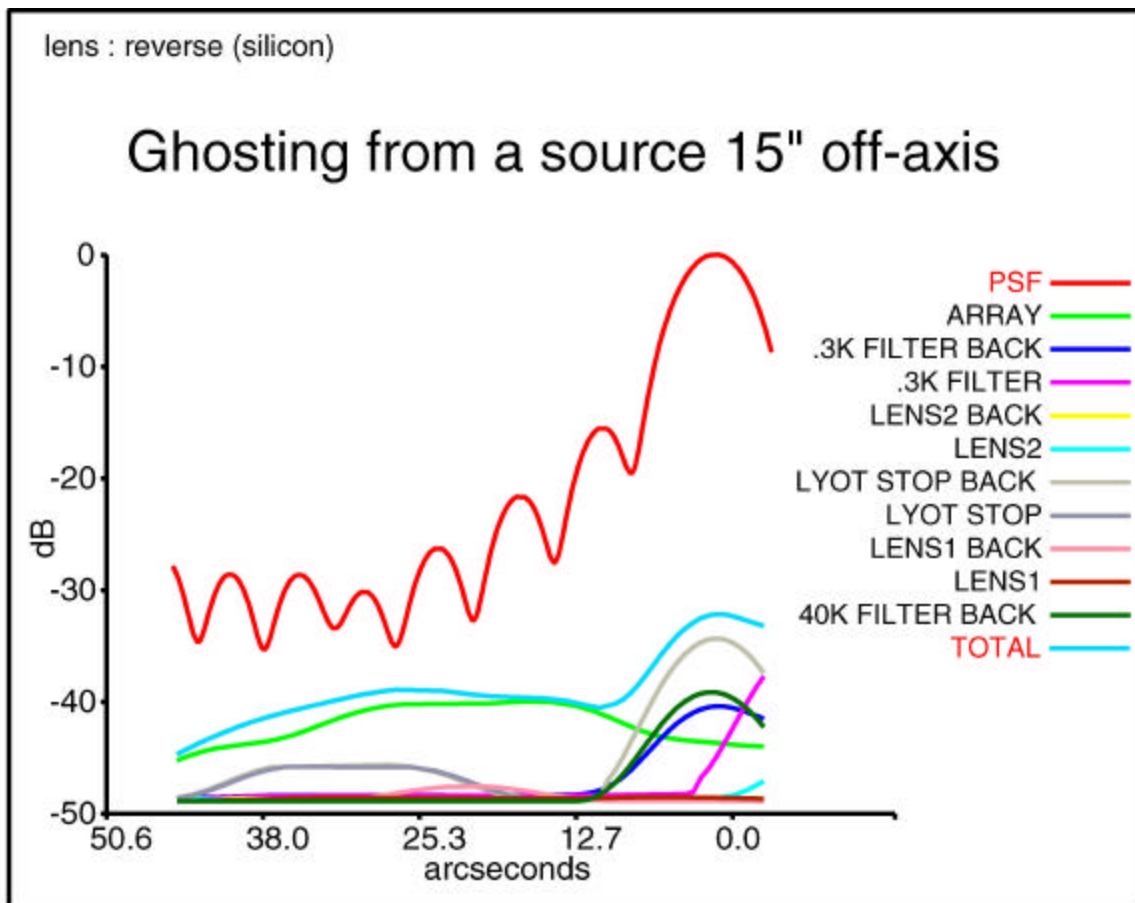
Figure 7. Ghost images created by reflections between pairs of surfaces. A PSF has been added to show that ghosting will not create any extra side lobes. Each line represents the image formed by light first reflected from a given surface.

Manufacture

A number of manufacturers have been found who can cut aspheric silicon lenses. Preliminary quotes have been of the order $3000 and cheaper manufacturers may be found once the final shapes are known. Due to thermal expansion, the parameters given to them will be slightly different from the parameters in the Appendix (which are what are required at cryogenic temperatures while the lenses are cut at room temperatures). Code V can calculate the differences.

The lenses are housed in an optics box mounted at the first lens only. Flexible cooling straps connect to the other stages. G10 tube connects the 40K and 3K parts, a 0.5 mil stainless steel foil makes this tube light-tight, and black baffles (a stycast/ silicon carbide paint) ensure stray light is absorbed. Again, the parts are cut at room temperatures to lengths calculated so that when they cool, the lenses/filters are apart by the lengths listed in the Appendix.
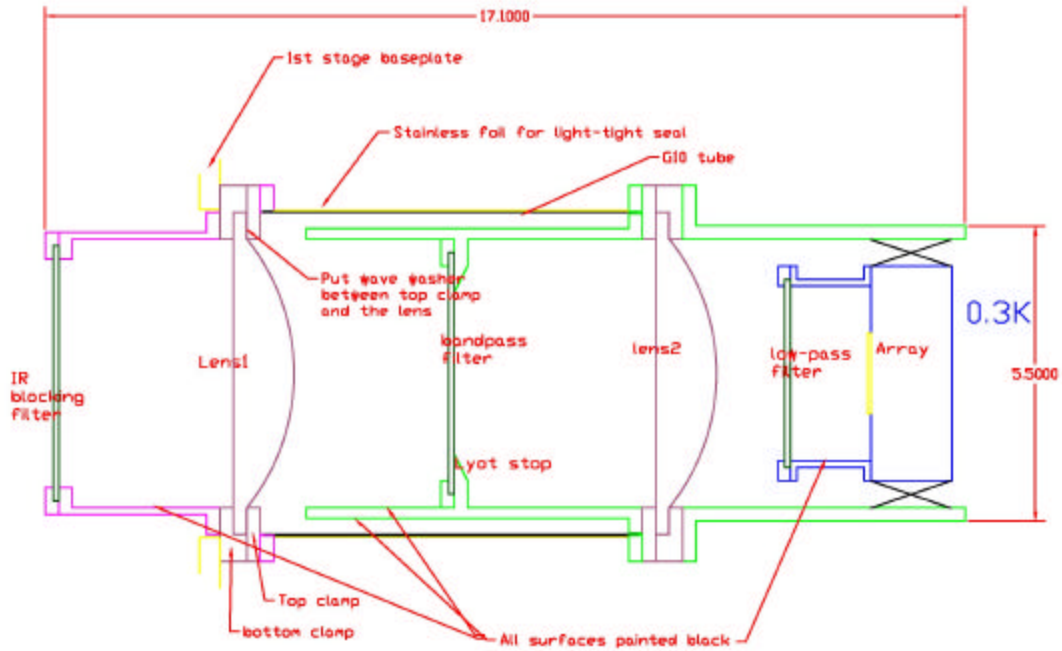
Figure 8 : The housing for a quartz version of the cold optics. The Silicon optics will have a similar housing. Sizes are in inches.

Conclusions

The silicon based optical design presented should produce diffraction limited beams across the entire 8×8 array, with pixel sizes of approximately 8? (taking into account finite detector size). Spillover and side lobes (either from diffraction or stray light) should be below -30 dB beyond 25? from the main beam). The First side lobes are -18 to -16 dB at around 11.7? from the main beam in line with what is to be expected with typical fast edge tapers in the illumination of a primary mirror. All in all the design looks good, it easily fits in the cryostat and it should be possible to make at reasonable cost.

Appendix

Listed below are the parameters of the lenses in sequence file format:

S <surface number> <surface curvature> <distance to next surface> <material>.

SLB <surface name>

K,A,B,C,D represent the terms of the aspheric formula which gives the sag z in terms of h (the distance from the

optical axis) and c (the curvature): $z = \dfrac{ch^2}{1+\sqrt{1-(1-K)c^2h^2}} + Ah^4 + Bh^6 + Ch^8 + Dh^{10}$

```
S 6    0.00000000    55.000000        'vac'
   SLB "Gregorian focus"


S 7    0.00000000    5.000000         'filter'
   SLB "40K filter"


S 8    0.00000000    76.525000        'vac'
   SLB "40K filter back"


S 9    0.00000000    14.083192        'silicon'
   SLB "lens1"


S 10   -0.00413441   94.170438        'vac'
   SLB "lens1 back"
   ASP
   K   -3.884782
   IC    YES      ;CUF   0.000000
   A -.184951E-08  ;B -.640385E-11  ;C 0.253747E-14  ;D -.267786E-18


S 11   0.00000000    5.000000         'filter'
   SLB "Lyot stop"


S 12   0.00000000    71.531369        'vac'
   SLB "Lyot stop back"


S 13   0.00000000    10.185237        'silicon'
   SLB "lens2"


S 14   -0.00467100   10.000000        'vac'
   SLB "lens2 back"
   ASP
   K   -12.413004
   IC    YES      CUF:   0.000000
   A 0.891879E-08  ;B -.142099E-09  ;C 0.992324E-13  ;D -.219622E-16


S 15   0.00000000    5.000000         'filter'
   SLB ".3K filter"


S 16   0.00000000    44.069873        'vac'
   SLB ".3K filter back"

 ARRAY
```

The Apertures have the following radii (130% clear aperture):

Filter 1	45 mm
Lens 1	65 mm
Lyot stop	23.8 mm
Lens 2	40 mm
Filter 3	40 mm